Journal of Molecular Liquids 453 (2026) 129530

Contents lists available at ScienceDirect

Journal of Molecular Liquids

journal homepage: www.elsevier.com/locate/molliq

Influence of different production processes on the formation of asolectin-based colloids to improve quercetin and rutin formulation efficiency☆

Virág Viktória Kiss [a], Norbert Varga [a,b], Ádám Juhász [a,b], László Seres [a,*], Edit Csapó [a,b,**]

[a] Interdisciplinary Excellence Center, Department of Physical Chemistry and Materials Science, University of Szeged, H-6720 Rerrich B. sqr. 1, Szeged, Hungary
[b] MTA-SZTE Lendület "Momentum" Noble Metal Nanostructures Research Group, University of Szeged, H-6720 Rerrich B. sqr. 1, Szeged, Hungary

ARTICLE INFO

Keywords:
Lipid particles
Soy phospholipids
Flavonoids
Encapsulation capacity
Microfluidics
Drug release

ABSTRACT

Poor stability and low bioavailability often hinder the application of flavonoids, despite their benefits. Integration of nanotechnology and flavonoid research has emerged as a cutting-edge approach to ensure the effective delivery and stabilization of these natural antioxidants. Lipid-based colloidal carriers are widely investigated for improving the solubility and bioavailability of bioactive compounds. In this work, quercetin (Que) and rutin (Rut), two structurally related flavonoids with distinct physicochemical properties, were encapsulated into asolectin (Aso)-based colloids using thin-film hydration, ethanol injection, and microfluidic preparation methods. The influence of formulation routes and drug-to-lipid mass ratios on particle size, ζ-potential, encapsulation efficiency (EE%), and drug loading (DL%) was systematically investigated. Formulations with hydrodynamic diameters below 150 nm and highly negative ζ-potentials were obtained for both flavonoid formulations, however, significant differences were observed in EE% and attainable DL%. Thin-film hydration was proved to be optimal for Que, yielding EE% > 90% and 10-fold increase in water solubility, while microfluidic preparation enabled dominantly higher DL% (~12%) for Rut without precipitation. *In vitro* release studies demonstrated enhanced dissolution of Que upon formulation, whereas Rut release remained largely diffusion controlled. The results highlight the critical role of unique molecular features and independent preparation methods in determining the performance of lipid-based flavonoid-containing delivery systems.

1. Introduction

Flavonoids are natural compounds found in various plants, including seeds, flowers, and barks, where they serve essential functions. These bioactive compounds belong to the category of secondary metabolites. They possess a characteristic structure composed of three rings, consisting of two phenyl groups and one pyran, also known as the benzo-γ-pyrone skeleton [1]. Flavonoids are a broad class of polyphenolic compounds that exhibit a wide range of biological activities, including antioxidant [2], anti-inflammatory [3], and anticancer effects. Among them, quercetin (Que) and rutin (Rut) have attracted considerable attention due to their potential therapeutic and nutraceutical applications [4–6]. Despite their promising bioactivity, the practical utilization of these compounds is strongly limited by their poor water solubility ($\log P_{Que} = 1.48–2.15$ [7] $\log P_{Rut} = -1.30–0.15$ [8]) low bioavailability, and unfavorable dissolution characteristics under physiological conditions [9]. Consequently, the development of efficient formulation strategies capable of improving their solubility and release behavior remains a major challenge [10,11]. One potential preformulation strategy for the above-mentioned limitations is the use of nanotechnology-based delivery systems [12], such as polymeric nanoparticles [13] or liposomes [14]. Additionally, the incorporation of these flavonoids into cyclodextrin complexes can also improve their water solubility and protect them from degradation [15,16]. Another approach involves using solid dispersion techniques, which can increase the dissolution rate and bioavailability of poorly water-soluble

☆ This article is part of a Special issue entitled: 'CPBCI 2025 Conference' published in Journal of Molecular Liquids.

* Corresponding author.
** Corresponding author at: Interdisciplinary Excellence Center, Department of Physical Chemistry and Materials Science, University of Szeged, H-6720 Rerrich B. sqr. 1, Szeged, Hungary.
E-mail addresses: seres.laszlo@chem.u-szeged.hu (L. Seres), juhaszne.csapo.edit@med.u-szeged.hu (E. Csapó).

https://doi.org/10.1016/j.molliq.2026.129530
Received 28 January 2026; Received in revised form 21 March 2026; Accepted 30 March 2026
Available online 1 April 2026

compounds [17].

Lipid-based carrier systems, such as liposomes and lipid nanoparticles, have emerged as versatile platforms for the encapsulation of hydrophobic and amphiphilic molecules [18]. These systems can enhance apparent solubility, protect labile compounds, and modulate release kinetics through molecular-level interactions between the encapsulated compound and the lipid matrix [19]. Asolectin (Aso), a naturally derived mixture of phospholipids, is particularly attractive as a cost-effective carrier material due to its biocompatibility, amphiphilic character, and ability to self-assemble into spherical colloidal structures in aqueous media [20,21]. The main components of asolectin – derived from soy bean – are phosphatidylcholine (PC) (35–45%), phosphatidylethanolamine (PE) (25–35%) also known as cephalin, phosphatidylinositol (PI) (10–20%), and smaller amounts of other lipids like phosphatidic acid (PA) (2–5%), where the first two components are zwitterionic, while the last two contains only negative charge [22]. The quality and quantity of the components may vary naturally depending on their origin and from the manufacturer who distributes it. Physicochemical properties of the encapsulated compound, including molecular size, polarity, and hydrogen-bonding capability, strongly influence the formation, stability, and loading capacity of lipid-based particles [23,24]. In addition to the composition, the preparation method plays a decisive role in determining the particle characteristics. Conventional lipid-based formulation approaches such as thin-film hydration [25] and ethanol or other solvent injection [26] differ significantly in solvent environment and self-assembly pathways [27], while microfluidic techniques [28] offer improved control over mixing conditions and particle formation [29]. Namely, the most decisive parameters of the thin-film hydration method are the lipid composition and concentration, but the evaporation rate and the hydration time and agitation also affect the characteristics of the formed liposomes. Moreover, the downsizing parameters like extrusion or sonication (time, pulse frequency, and power) are critical to reach the desired size [25]. For ethanol injection method, the injection velocity and the stirring speed plays a key role in size regulation, but the lipid and the organic solvent concentrations are also determinative parameters to avoid destabilizing the newly formed bilayers [26]. In case of the microfluidic preparation method, probably the most important parameter is the flow rate ratio (FRR, the ratio of water to organic solvent), the total flow rate (TFR), but the geometry of the mixer is crucial. In this case very high lipid concentrations can lead to channel clogging or increased polydispersity index (PDI) [28].

To the best of our knowledge, comparative studies evaluating these mentioned preparation methods for flavonoid encapsulation under consistent conditions are still limited, which is the main motivation of our research. Some liposomal formulations are already commercially available, but due to the liposomal technology, these products fall into the premium category, making their prices noticeably higher than traditional formulations. Accordingly, we used an inexpensive and easily accessible soy lecithin derivative (also called asolectin, Aso) to fabricate Que- and Rut-loaded liposomal particles by using thin-film hydration, ethanol injection, and microfluidic techniques. The effects of formulation method and drug-to-lipid mass ratio on particle size, surface charge, EE%, and DL% were systematically investigated. Furthermore, molecular interactions were analyzed using thermal and spectroscopic techniques, and the *in vitro* release behavior of the flavonoids from the carriers was also evaluated. Although Que and Rut are structurally related flavonoids, the presence of a disaccharide moiety in Rut leads to substantial differences in water solubility, molecular interactions, and formulation behavior. A systematic comparison of the formulation of these compounds into lipid-based carrier systems can provide valuable insights into a deeper understanding of structure-property relationships and the cost-effective design of more advanced formulations, as these compounds are potential ingredients in modern pharmaceutical and nutritional supplement products due to their antioxidant and anti-inflammatory properties [30–33].

2. Materials and methods

2.1. Materials

Soy phospholipids (phospholipid mixture (asolectin) Aso, ≥ 20% phosphatidylcholine (PC) content), chloroform ($CHCl_3$ > 99.8%), quercetin hydrate (Que, $C_{15}H_{10}O_7 \times x\ H_2O$ > 95%;), rutin hydrate (Rut, $C_{27}H_{30}O_{16} \times x\ H_2O$, ≥ 94% (HPLC)), dipalmitoylphosphatidylcholine (DPPC, > 99%) and cellulose dialysis membrane ($M_{w\ cut\text{-}off}$ = 14,000) were obtained from Sigma Aldrich Hungary. Methanol (CH_4O, 99.99%), ethanol (C_2H_6O, 99.99%), sodium chloride (NaCl, ≥ 99%), sodium phosphate dibasic dodecahydrate ($Na_2HPO_4 \times 12\ H_2O$; ≥ 99%), sodium phosphate monobasic dihydrate ($NaH_2PO_4 \times 2\ H_2O$; ≥ 99%) were obtained from Molar Chemicals Kft. Tween-80 (Polyoxyethylene (20) sorbitan monooleate, 99%) was obtained from Reanal Kft. Highly purified water (MQ water) was obtained by deionization and filtration with a Millipore purification apparatus (18.2 MΩ·cm at 25 °C). All solvents and reagents (except Aso for the ethanol injection and microfluidic method) were of analytical grade and no further purifications were made. The purification of Aso was carried out as written in *Section 2.2.2*.

2.2. Methods

2.2.1. Preparation of Que-containing particles with the thin-film hydration method

25 mg of unpurified Aso was weighed into a round-bottom flask, which was dissolved in 2.5 mL of a 9:1 (*V*/V) mixture of chloroform ($CHCl_3$) and methanol (MeOH). To obtain 1:20, 1:40, and 1:200 Que:Aso mass ratios, Que was dissolved in MeOH beforehand (5 mg/mL) and was added to the $CHCl_3$ solution in different portions (250, 125, and 25 μL, respectively). Pure MeOH was added to this mixture to obtain the final 9:1 $CHCl_3$:MeOH ratio. In the case of higher mass ratios (1:10 and 1:2), Aso and Que were measured directly into the round-bottom flask and dissolved in the solvent mixture. Then the solvent was evaporated with a rotary evaporator (IKA RV 116 05-ST, 100 rpm, 50 °C, 10 min), which resulted in the formation of a Que-Aso film on the wall of the round-bottom flask. This film was then hydrated with 25 mL of MQ water, stirred for 10 min, and sonicated for 10 min. The sonication time was determined by **Fig. S1A,** according to which the PDI value of the dispersion does not change significantly after 10 min. Although the size of the particles continues to decrease after this time interval (further sonication would have risked "shaking out" the encapsulated drug from the particles). Moreover, a narrower size distribution of the particles, with a likely liposomal structure, (**Fig. S1B**) also achieved this way.

2.2.2. Preparation of Rut-containing particles with the thin-film hydration method

Rut-containing dispersions were prepared similarly to the Que-containing ones (*see Section 2.2.1.*). In this case, the MeOH contained Rut in 25 mg/mL concentration to obtain 1:40, 1:20, 1:10, 1:5, and 1:4 Rut-to-Aso mass ratios. For the 1:2 mass ratio, solid Rut and unpurified Aso were directly measured into the round-bottom flask and dissolved in a $CHCl_3$:MeOH 9:1 mixture. The evaporation of the solvent and the hydration of the lipid film were carried out exactly like in the case of Que to form liposomal formulation of Rut.

2.2.3. Purification of Aso

Since the unpurified Aso did not dissolve completely in ethanol, the removal of the ethanol-insoluble lipids (like phosphatidylinositol and other lipids present in small proportions) was necessary to investigate the applicability of the ethanol injection and microfluidic preparation methods [34,35]. The extraction of ethanol-soluble components is well-known and widely applied technique, and as a result, the phosphatidylcholine (PC) content of asolectin isolated from the soybeans used can be significantly increased [34,35]. To carry out this experiment, roughly 9.5 g of unpurified Aso was taken into a Duran bottle and 85 mL of

absolute ethanol was poured on it, which was followed by 1 h of sonication (37 kHz). After the sedimentation of the ethanol-insoluble phase, the supernatant was removed and filtered through a 0.45 μm Teflon filter to get rid of any insoluble Aso residues. Then the pure brownish solution was evaporated by a rotary evaporator similarly to the lipid films in the former section. As a result, we obtained a brownish, soft material with a yield of ~23%, in which the PC content, as expected [36], increased to ~60% from the initial ~20% (20% is based on manufacturer data) determined by differential scanning calorimetry (DSC) measurements [37,38]. For the solvent injection and microfluidic particle formation methods, this purified Aso (pAso), which was stored at −20 °C, was used.

2.2.4. Preparation of Que-containing particles with the ethanol injection method

25 mg of pAso was dissolved in 5 mL of ethanol, and this solution was added dropwise to 5 mL of MQ water. In the case of the Que-containing samples, the ethanolic solution contained the Que to obtain 1:20, 1:40, and 1:200 Que:Aso mass ratios (0.25, 0.125, and 0.025 mg/mL, respectively). In the case of the optimal 1:20 mass ratio, 1.65 mL of ethanolic solution was added dropwise to 5 mL of MQ water under magnetic stirring (500 rpm).

2.2.5. Preparation of Rut-containing particles with the ethanol injection method

Ethanolic stock solutions of pAso (20 mg/mL) and Rut (20 mg/mL) were prepared first. Secondly, titrating solutions were made by measuring 0.5 mL of pAso stock solution and given amounts (12.5, 25, 50, 100 and 125 μL) of Rut stock solution complemented to 1 mL of final volume with pure ethanol to obtain 1:40, 1:20, 1:10, 1:5 and 1:4 Rut: lipid mass ratios. We added these solutions with a volume of 0.5 mL to 5 mL of MQ water (1:10 ethanol:water ratio ($V_{EtOH}/V_{MQ} = 0.1$)) under 500 rpm of stirring rate to obtain Rut-containing formulations.

2.2.6. Preparation of Rut-containing particles with the microfluidic method

For the preparation of Rut-containing particles, a Syrris Asia Flow Syringe Pump System (Syrris Ltd.) was also used. Based on solubility problems the fabrication possibility of only the Rut-based formulations was tested by flow conditions. During these studies the same stock and sample solutions were prepared as for the ethanol injection method in 2 mL of final volume. During the studies 3 different flow channels were used: 2 of them (*ch1*, *ch2*, ν_{MQ1}, ν_{MQ2}) were used to flow the MQ water at a defined rate (250 μL/min for each pump, $\Sigma\nu_{water} = 500$ μL/min) and the 3rd (*ch3*, ν_{EtOH}) was used for the ethanolic Rut-Aso solution. The flow rate of this ethanolic solution was changed (16.6 μL/min – 250 μL/min) during the preparation, as Table 1 shows. These 3 channels were directed into a T-shaped junction in which the solutions were mixed. In channel 4 (*ch4*) the particle formulation was directed into a container.

2.2.7. Purification of the formulations

The purification of the particles was carried out as follows: 5 mL of the prepared dispersions was taken into a dialysis bag ($M_{w\ cut\text{-}off} = 14{,}000$), which was inserted into 500 mL of MQ water. The dialysis time was determined by following the hydrodynamic radius, ζ-potential, EE %, and DL% values of the particles as presented in **Fig. S2.** In the case of the thin-film hydration and ethanol injection methods for Que, the samples were purified with gel filtration: 2 × 500 μL Sephadex G-50 gel was taken into an Eppendorf tube and centrifuged at 13000 rpm for 5 min. Onto these, 500 μL of sample was taken to be centrifuged for 6 min at 6000 rpm. When solid samples were needed, the purified samples were frozen, lyophilized overnight (Christ Alpha 1–2 LD) and stored at −20 °C.

Table 1
The applied flow rate values on the individual channels (*ch1-ch3*) for the preparation of particles with the microfluidic method.

ch1 ν_{MQ1} (μl/min)	***ch2*** ν_{MQ2} (μl/min)	***ch3*** ν_{EtOH} (μl/min)	ν_{water}/ν_{EtOH}
250	250	250	2
250	250	166	3
250	250	100	5
250	250	83.3	6
250	250	62.5	8
250	250	50	10
250	250	33.3	15
250	250	25	20
250	250	16.6	30

2.2.8. Characterization of the particles

Dynamic light scattering (DLS) and ζ-potential (electrophoretic light scattering) measurements were carried out with a HORIBA SZ-100 NanoParticle Analyzer (HORIBA Jobin Yvon, Longjumeau, France), equipped with semiconductor laser (λ = 532 nm, 10 mW) as light source and a photomultiplier detector for the quantification of scattered intensity at 90° scattering angle. In every case, stable laser signal (5 s of stabilization) and at least 1000 kCPS count rate was achieved during 30 s of accumulation time to obtain stable correlation functions. For the conversion of electrophoretic mobility to ζ-potential, the Smoluchowski-model was used. As a result, hydrodynamic diameter, the size distribution, and the ζ-potential of the particles could be measured. The results are the averages of 5 measurements.

Differential scanning calorimetry (DSC) was used to characterize the purified and unpurified Aso; Que, Rut and the solid formulations. DSC curves of the samples were recorded with a Mettler-Toledo 822e calorimeter between 25 and 500 °C using a 5 °C/min heating speed and 50 mL/min N_2 flow. The results were evaluated with a STARe 12.10 software. DSC studies were used to determine the PC lipid-content of the purified Aso. Namely, DSC curves of dipalmitoylphosphatidylcholine (DPPC), as a standard PC source, were registered using different DPPC contents (0–6.0 mg), and in the range of 250–350 °C we calculated the decomposition enthalpies (ΔH) (derived from the integrated heat flow values; $\Delta H = K \times F_{peak}$, where *K* is the corresponding adjustment factor, F_{peak} is the peak area). These enthalpies were plotted as a function of the DPPC amount to create a calibration curve.

Fourier-transform infrared (FT-IR) spectra were registered with a Thermo Scientific Nicolet™ Summit™ FTIR Spectrometer, equipped with an ATR measurement head (ZnSe). Besides the pure Aso and drugs, the formulations were recorded, as well. The samples were freeze-dried before the measurement, which was carried out at the 500–4000 cm^{-1} range with 1 cm^{-1} resolution with the average of 16 interferograms.

2.2.9. Determination of encapsulation efficiency (EE%), drug loading (DL %) and in vitro release studies

In the case of the drug containing particles, the determination of EE% and DL% was performed with the help of a JASCO V-770 UV–VIS spectrophotometer. In short, the lyophilized drug-containing particles were redispersed in methanol (for Que) or in ethanol (for Rut) using 10 min of sonication. After this, the samples were stirred for 2 h and centrifuged for 10 min at 10,000 rpm to get rid of the undissolved materials. The UV-VIS spectra of the solutions were registered in the 200–500 nm range, and the absorbance of the drugs was determined at $\lambda_{max\ Que} = 371$ nm and $\lambda_{max\ Rut} = 363$ nm with the use of pre-made calibration curves (**Fig. S3**) The EE% and DL% values were calculated with the following equations.

$$EE\% = \frac{encapsulated\ mass\ of\ drug}{total\ mass\ of\ drug} \bullet 100 \quad (1)$$

$$DL\% = \frac{encapsulated\ mass\ of\ drug}{total\ mass\ of\ nanoparticles} \bullet 100 \quad (2)$$

Before the *in vitro* release measurements, 5 mL of the dispersions was taken into a dialysis membrane, which was inserted into 35 mL of

physiological PBS solution (pH = 7.4, 0.9% NaCl), which also contained 2.5 mg/mL Tween80 surfactant to enhance the dissolution of the poorly water-soluble drugs. During the dissolution studies, the UV-VIS spectra of the released drugs were recorded in the 200–500 nm wavelength range, and the absorbance at the absorption maximum ($\lambda_{max\ Que}$ = 376 nm and $\lambda_{max\ Rut}$ = 364 nm) was converted into concentration with the help of calibration curves (**Fig. S4**) to calculate the percentage of the dissolved drug. The measurements were carried out at 37 °C. The dissolution profiles were fitted with different kinetic curves (first order, Korsmeyer-Peppas, Higuchi, and Weibull models) [39].

3. Results and discussion

To achieve the encapsulation of Que and Rut into lipid-based carrier particles, different formulation methods were tested and analyzed. These methods have different features and experimental designs, which can determine the main characteristics of the systems (particle size, ζ-potential, encapsulated amount of the drug, *etc.*), and the structural difference between the drugs can also strongly influence the results of the preparations. To overcome these problems as well as to compare the formulations with each other, we varied the drug-to-Aso mass ratio (m_{drug}:m_{Aso}) in the same way for all formulations.

3.1. Preparation and characterization of the Que-containing particles

3.1.1. Preparation of the formulations containing Que with the solvent injection method

In the first step, we studied the effectiveness of the ethanol injection process on the formability of the individual formulations. To evaluate the dominant effect of pAso concentration on the size and structural features of the drug-free and drug-loaded formulations, the Aso- and Que-Aso-containing ethanolic solutions were added dropwise to MQ water, and the hydrodynamic diameter of the created particles at increasing Aso concentration was measured with DLS (after 5 min stirring) (Fig. 1A, B). It can be seen on Fig. 1A that the continuous addition of the lipid solution into water results in the formation of particles with nearly same size for drug-free formulations (d ~ 115 nm) to c_{pAso} = 1.24 mg/mL and constantly increasing values for drug-containing systems (d ~ 150 nm at c_{pAso} = 1.24 mg/mL). This difference in size at the same lipid content could indicate the presence of Que in the formulations. Fig. 1B represents the measured hydrodynamic diameter of the formulations at chosen Que-to-pAso mass ratios. We can conclude that the Que content increases the size of the particles (from 140 nm (m_{Que}:m_{pAso} = 1:200) to 174 nm (m_{Que}:m_{pAso} = 1:200).

Our opinion is that the hydrophobic Que molecules are preferentially incorporated into the lipid bilayer(s), instead of the inner aqueous core, increasing the size of the formulation. Chemically, Que is a hydrophobic polyphenol, but functionally it exhibits amphipathic properties, as it can position itself at the lipid-water interface. In biological systems, it behaves as amphipathic ligand when incorporated into the cell membrane. With its hydrophobic rings, it turns toward the interior of the membrane, while with its -OH groups, it interacts with the aqueous medium on the membrane's surface and positions itself at the lipid-water interfaces. Fig. 1C shows that the ζ-potential values change a very small extent with the drug-to-pAso ratio (from −43.5 mV to −57.8 mV). This *ca.* 14 mV decrease could be due to the incorporation of the Que into the liposomes – as mentioned above –, which could stabilize the particles. More stable colloidal particles cause a greater absolute ζ-potential (a more negative

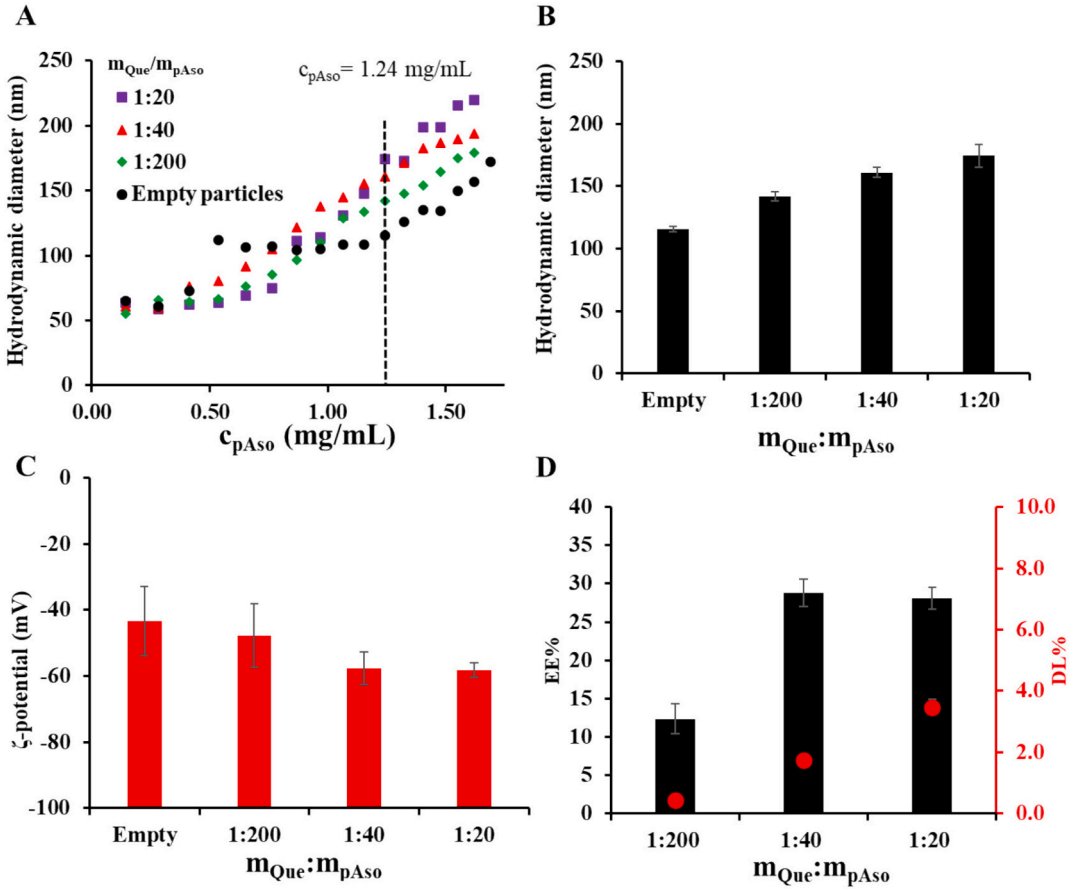

Fig. 1. (**A**) Change of the hydrodynamic diameter of the formed drug-free and Que-loaded lipid-based formulations at different pAso concentrations and for several Que-to-pAso mass ratios. Hydrodynamic diameters (**B**), ζ-potential values (**C**), and EE% (columns) and DL% (●) (**D**) of the formulations at various Que-to-pAso mass ratios (c_{pAso} = 1.24 mg/mL, $V_{MQ\ titrated}$ = 5 mL).

value in our case). Moreover, the pK_{a1} of Que (ring A/7-OH) is at around 6.6 [40], which suggests that in MQ water (pH ≈ 6–7) Que molecules are partly deprotonated obtaining a negative charge. Incorporation of components with a negative charge into the lipid bilayers may contribute to the formation of a more negative ζ-potential. From the point of view of the amount of drug formulated into the particles (Fig. 1D), relatively small EE% values could be observed (EE% = 12.4, 28.8, and 28.1% for the 1:200, 1:40, and 1:20 mass ratios, respectively), which could be due to the presence of ethanol in the formulations. Ethanol enhances the solubility of the drug in the medium, which prevents its enrichment in the particles. Based on it, the DL% < 4%. We can conclude that this process is not particularly effective for formulating the active ingredient Que into pAso-based lipid formulations.

3.1.2. Preparation of the formulations containing Que with the thin-film hydration method

During this method, lipid films with different drug contents were formed on the wall of round-bottom flasks, which were hydrated with MQ water to produce particle dispersions. Stirring and ultrasonic treatment for 10–10 min were applied to promote particle formation and control their size. The duration of the sonication was determined by time-dependent measurements (**Fig. S1**), which indicated that 10 min of ultrasonic treatment is eligible for creating particles with good PDI values (~ 0.3) and appropriate size. Moreover, these 10 min are enough to avoid the risk of destroying the particles or the possibility of decreasing the amount of encapsulated drug content as well. As it can be seen on **Fig. S1** the after 60 min of sonication, the lipid-based formulation is already damaged, as indicated by the large error in the measurement.

As Fig. 2A presents, the size of the empty carriers is around 150 nm, which is somewhat larger than that obtained for the ethanol injection technique. This variance could naturally stem from the difference in techniques, but it could also originate from the fact that we used unpurified Aso during this process, which contains significantly more components. To decide which is preferred, experiments for the formation of drug-free liposomes were also carried out with the pAso as well using the TFH technique, and as **Fig. S5** represents, particles of ~ 120 nm could be prepared. This indicates that the difference of the particle sizes would stem from the lipid composition rather than the preparation method.

In presence of Que interesting results are obtained. The Que content of the formulations varied between 1:200 and 1:20 Que:Aso mass ratios (from 0.005 to 0.05 mg/mL) and the hydrodynamic size, ζ-potential, EE % and DL% values were determined for the formulations as Fig. 2 shows. In the case of the smaller Que contents (m_{Que}:m_{Aso} = 1:200 to 1:20), the diameter of the particles varies between 142 nm and 101 nm, and it can also be stated that due to the incorporation of the drug into the carriers, more compact particles with smaller sizes can be created (Fig. 2B).

This observation is contrary to what is experienced when using ethanol injection technique and can be attributed to several biophysical phenomena. When incorporated the Que molecules into the lipid bilayer, they tend to localize in the interfacial region (between the polar headgroups and the hydrophobic acyl chains). The insertion of Que alters the packing parameter (P) of the lipids. By occupying the voids between phospholipid molecules, Que can induce a positive membrane curvature, which energetically favors the formation of smaller vesicles

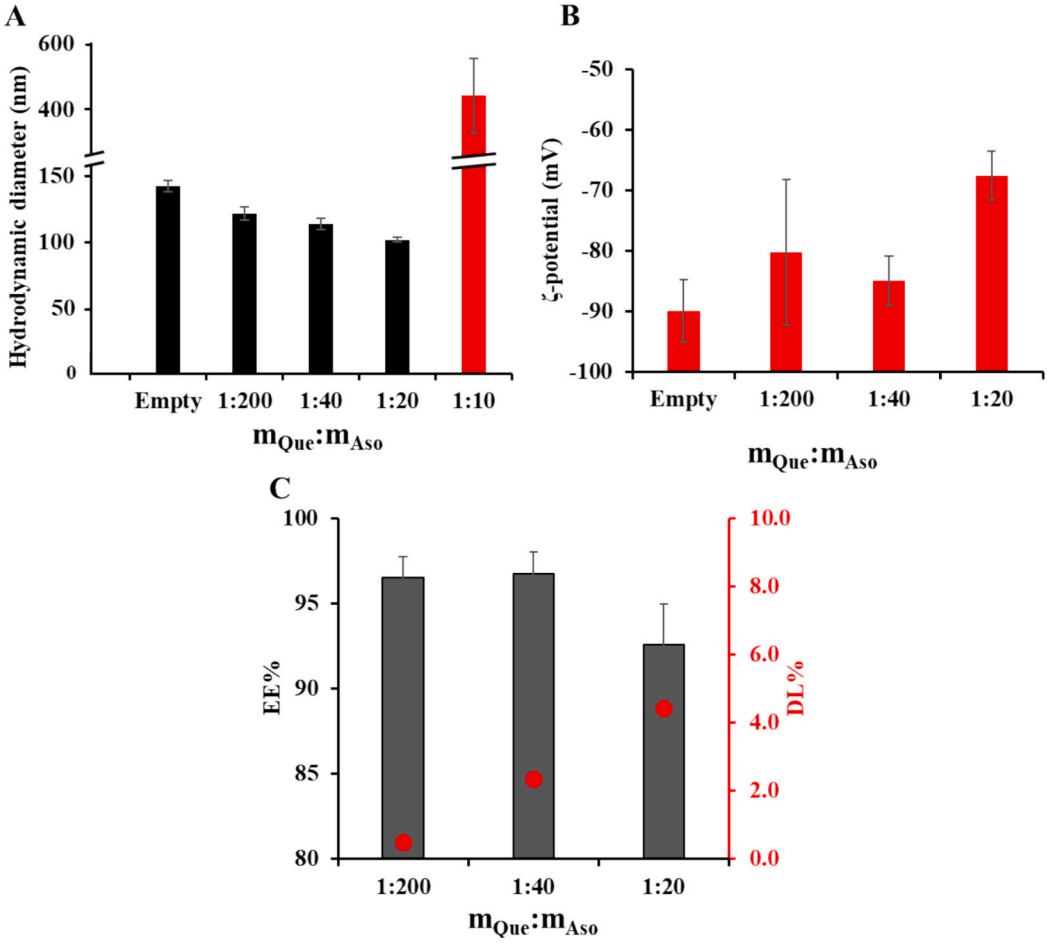

Fig. 2. The (**A**) hydrodynamic diameter, (**B**) ζ-potential and (**C**) the EE% (columns) and DL% values (●) of the formulations at different Que-to-Aso mass ratios created by thin film hydration method (c_{Aso} = 1 mg/mL, $V_{MQ\ final}$ = 25 mL).

with a higher surface-to-volume ratio during the hydration step. Moreover, Que has been shown to mimic the behavior of cholesterol in phospholipid bilayers. At specific concentrations, Que exerts a condensing effect, increasing the molecular packing density and decreasing the cross-sectional area per lipid. This increased cohesion within the bilayer can limit the uncontrolled growth of vesicles during film detachment, resulting in a more constrained, smaller particle size. During the transition from a dry lipid film to hydrated vesicles, the lipid sheets must "bridge" and close to shield their hydrophobic tails from water. Que may act as an edge-actant, reducing the line tension at the boundaries of the opening lipid bilayers. By stabilizing these edges during the fragmentation of the lipid film, the system can support the formation of a larger number of smaller vesicles rather than a few large, thermodynamically unstable ones. The presence of Que within the dry lipid film can interfere with the long-range van der Waals forces and hydration repulsion between adjacent bilayers. High Que concentrations may prevent the formation of large, multi-lamellar structures (MLVs) by promoting the budding or shedding of outer layers into smaller, oligo- or uni-lamellar vesicles (LUVs/SUVs) as soon as water penetrates the film.

Higher Que contents (m_{Que}:m_{Aso} = 1:10 and 1:2) were also tested as well, but in these cases even the film formations were not successful, and after hydration no reliable particle size values could be measured. Regarding the ζ-potential (Fig. 2B) of the particles, we can observe that relatively high negative ζ-potential values (from −89.9 mV to −71.5 mV) can be measured for all samples, which suggests that stable particles are formed with this method; however, trend-like changes in the values cannot be observed if we take the errors into account.

If we compare the EE% values with those determined for the ethanol injection technique – at the same Que:Aso ratios – we can state that higher EE% values (Fig. 2C) can be achieved (92–96%). This observation is based on the lack of ethanol and during this experiment the non-cleaned Aso was used, which contains more types of lipids. Under these conditions, the drug is located dominantly in the more hydrophobic carrier particles than in an aqueous medium, and the presence of other lipids also enhances the formulation of Que. Also, the DL% values show monotonous increase with the increase of the Que content of the formulations (0.48%, 2.36% and 4.42% for the 1:200, 1:40 and 1:20 mass ratios). With this method, the solubility of Que increased to 4.83 μg/mL, 24.2 μg/mL and 46.3 μg/mL respectively, which means 1.84, 9.20 and 17.6 times solubility increment compared to the solubility of Que in water at 25 °C (2.63 μg/mL [41]). Although the solubility increment (almost 20 times) at the 1:20 sample seems very promising, it needs to be noted that this high amount of drug cannot be held in solution for a long time. The formulation is stable for some hours after preparation, however a part of Que usually sediments by the following day. In contrast, the sample with a mass ratio of 1:40 remained stable even after several days, so we characterized the formulation produced at this ratio in detail.

3.2. Preparation and characterization of the Rut-containing particles

3.2.1. Preparation of the formulations containing Rut with the solvent injection method

The encapsulation of this less hydrophobic molecule was carried out with the same formulation methods as for Que mentioned earlier. Firstly, the ethanol injection method was tested. The same ethanol addition steps (Fig. 3A) were done as for Que to observe how the change of the drug affects the formation of the particles. For this, the same and –

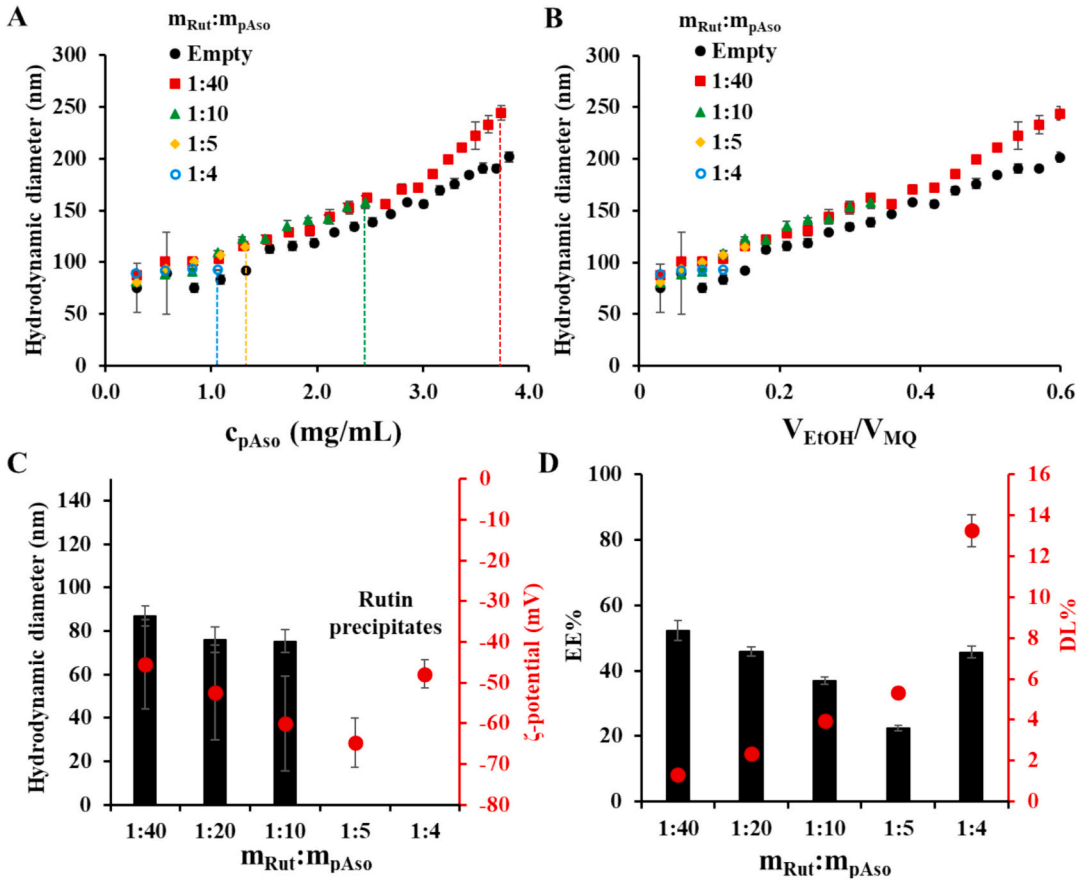

Fig. 3. Change of the hydrodynamic diameter of the formed drug-free and Rut-loaded lipid-based formulations at different pAso concentrations (**A**) and at various $V_{EtOH}/V_{MQ\ water}$ ratios (**B**) in the case of several Rut-to-pAso mass ratios. The hydrodynamic diameter (columns) and the ζ-potential values (●) (**C**), and the EE% (columns) and DL% (●) (**D**) of the formulations at various Rut-to-pAso mass ratios (c_{pAso} = 0.91 mg/mL, $V_{MQ\ titrated}$ = 5 mL).

when it was possible – higher drug:pAso mass ratios were analyzed. We can see that quite similar trends can be observed in the case of Rut as for Que: the more lipid is present in the system, the higher the particle size is (**Fig. 1A** and **3A**); however, the change of Rut content does not vary the diameter of the particles significantly. In this system, there is actually a very slight decrease compared to the increase in size observed in the case of Que, which is likely because the Rut molecules can also be located within the inner aqueous core of the lipid particles. The vertical dashed lines represent the precipitation of the drug molecules from the samples (in the order from 1:4 to 1:40). From the point of view of the solvent composition (Fig. 3B), the same increasing trend can be seen, and according to this, a 1:10 ethanol:water ratio ($V_{EtOH}/V_{MQ} = 0.1$) was chosen to carry on with. As Fig. 3C shows, particles at around 80 nm can be prepared and with good stability ((−45 mV)–(−60 mV)), however after purification, Rut from the 1:5 and 1:4 mass ratio samples precipitates. Regarding the trapped amount of Rut as presented in Fig. 3D, we can see an increasing trend in the DL% values up to 3.95% despite the decrease in the EE% values (53.3–36.9% for 1:40–1:10 samples). We can also say that in the case of Rut we could reach higher drug:lipid mass ratios (for Rut, maximum 1:10) than in the case of Que (for Que, maximum 1:20) resulting a somewhat higher DL% (~5% instead of ~3.8%). This can be explained by the fact that Rut is a slightly more water-soluble molecule and can also accumulate in the inner aqueous compartment of lipid particles, as it was mentioned above. Although the ζ-potential, EE% and DL% values could be determined for the 1:5 and 1:4 samples, they should not be considered reliable when discussing trends due to the precipitation of Rut in these samples.

3.2.2. *Preparation of the formulations containing Rut with the thin-film hydration method*

The encapsulation of Rut was carried out with the use of thin-film hydration method as well, in the hope of achieving as promising result as in the case of Que. For this – and to be parallel with the ethanol injection method for Rut – samples within the 1:40–1:4 Rut:Aso mass ratio range were prepared (according to *Section 2.2.2.*). As Fig. 4A shows, particles of 98–115 nm can be prepared, which is slightly higher than the ones produced by the ethanol injection method. With this preparation protocol, we could reach the 1:10 drug:Aso mass ratio – just like with the ethanol injection method –, which is higher than the ones with the particles for Que prepared with the thin-film hydration method under the same conditions. However, higher Rut content (1:5 and 1:4) could not be reached due to the precipitation of the drug, similarly to the ethanol injection method (Fig. 3A).

This way of preparation enables the production of stable particle dispersions in the 1:40–1:10 Rut:Aso mass ratio range, which is also indicated by the ζ-potential values (~ −65 mV).

The EE% values (Fig. 4B**)** are very similar to those of the ethanol injection method, showing a decreasing trend with the increase of the Rut content; only at the 1:10 composition can we see a slight difference (47.2% for the thin-film hydration and 36.7% for the ethanol injection method). In contrast, the DL% increases monotonously with the drug content, reaching 4.5% at the 1:10 mass ratio. The EE% and DL% are unreliable for the highest mass ratio values due to the precipitation of Rut. If we compare the EE% and DL% values with the Que-containing samples using the same thin-film hydration process, we can state that the EE% is measurably lower and the DL% is also less (DL% for Que at a 1:20 ratio is >4%, while for Rut at a 1:20 ratio the DL% is ~2.5%). This is due to the fact that in an aqueous medium the Rut is more soluble (based on logP values presented in the Introduction) than the Que. This means its accumulation in the formulation is less significant.

3.2.3. *Preparation of Rut-loaded particles with the microfluidic method*

In traditional methods, lipids often assemble into heterogeneous, multi-layered structures that require the use of harsh physical force (sonication or extrusion) to reach the desired size which limits the applicability of traditional methods in the production of delicate lipid-based systems such as those used in drug delivery. To overcome these disadvantages, a microfluidic method was also tested for Rut encapsulation. Comparing the experimental results obtained regarding the formulation of Que and Rut, we found that we can achieve a higher drug-to-Aso ratio (1:10) with Rut. Therefore, – also to avoid aggregation in the cell – we only attempted the formulation of Rut using this flow method.

For this, the same drug and lipid solutions were prepared as in the case of the ethanol injection method. As Fig. 5A shows, the increase of the pAso concentration – which also means the increase of the flow rate of the ethanol (Fig. 5B and Table 1) – the particle size increases significantly (form 132 nm to 236 nm).

If Rut is also present in the system, the particle size also varies significantly in the case of the Rut:pAso = 1:40 mass ratio. It can be seen that above $V_{water}/V_{EtOH} = 10$ the size does not change dominantly, moreover, to be parallel with the ethanol injection method, we chose the same $V_{water}/V_{EtOH} = 10$ (1:10 ethanol:water ratio) solvent composition to continue our experiments with. With these experimental parameters, the preparation of Rut-containing particles was carried out. We can see that the drug content does not change the size of the particles significantly even at the higher drug:lipid mass ratios after purification (Fig. 5C). Moreover, compared to the ethanol injection method, a higher average hydrodynamic diameter can be achieved (*e.g.*, at the Rut:pAso = 1:10 mass ratio, d = 75.4 ± 5 nm with the ethanol injection, and d =

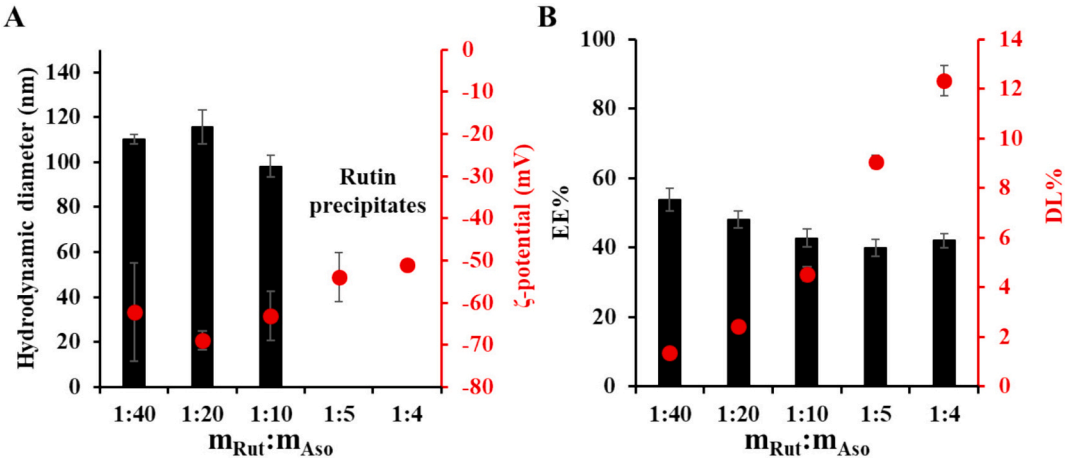

Fig. 4. The (**A**) hydrodynamic diameter and ζ-potential and (**B**) the EE% and DL% values of the formulations at different Rut contents created with the thin-film hydration method (c_{Aso} = 1 mg/mL, $V_{MQ\ final}$ = 25 mL).

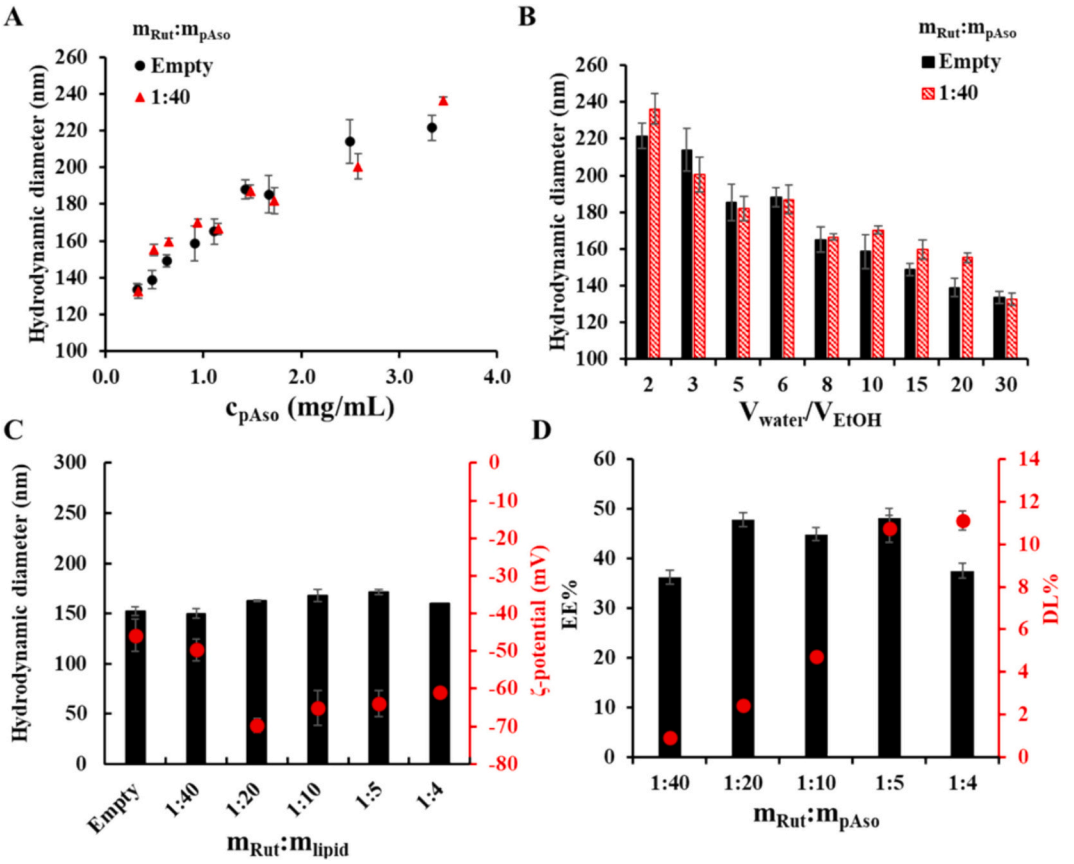

Fig. 5. Change of the hydrodynamic diameter of the formed drug-free and Rut-loaded lipid-based formulations at different pAso concentrations (**A**) and at various $V_{MQ\ water}/V_{EtOH}$ ratios (**B**) in the case of Rut-to-pAso 1:40 mass ratio. The hydrodynamic diameter (columns) and the ζ-potential values (●) (**C**), and the EE% (columns) and DL% (●) (**D**) of the formulations at various Rut-to-pAso mass ratios after purification (c_{pAso} = 0.91 mg/mL).

168 ± 6 nm with the microfluidic method). Based on this size increase, we initially assume that more active ingredients can be formulated, because the lipid composition is the same; however, the preparation ways are different. It was also confirmed that samples prepared at 1:5 and 1:4 mass ratios show higher stability (without precipitation of the drug), which is an improvement compared to the ethanol injection method. This increase in stability is confirmed by the ζ-potential values, which varied between −49.7 mV and − 69.8 mV. Regarding the drug content of the particles (Fig. 5D): EE% values between 36.2% and 48.0% could be achieved, however, no well-observable trend can be stated. For the DL% values the same increasing trend can be seen as for the other preparation methods, however, in this case DL% = 11.1 ± 0.4% could be measured, which is a promising value compared to the other preparation methods (DL% ~ 2.5–4%).

A comparative table summarizes all the production protocols with advantages and limitations and the characteristics of the formulations (Table 2).

As it can be seen, for Que, the application of the TFH technique is more preferred because high EE% and improved Que water solubility can be achieved, and the size of the colloids is also smaller. For Rut, the highest drug-to-lipid ratio can be achieved by using the MF method, which results in a higher DL% (~ 11%) with a 160-nm particle size.

3.3. Characterization of the chosen formulations

Comparing the formulation results with the active ingredients, we characterized the most promising formulations in both molecules. For this, we chose the thin-film hydration method for Que (m_{Que}:m_{Aso} = 1:40) and the microfluidic method for Rut (m_{Rut}:m_{pAso} = 1:4) to fabricate drug-loaded colloidal particles. As the first step of the characterization of these formulations – besides the determination of the average diameters, ζ-potentials, EE%, and DL% values mentioned in Chapter 3.1

Table 2
The applied production protocols with the characteristics of the formulations.

Preparation method	Drug	Optimal ratio (drug:lipid)	Particle size (nm)	ζ-potential (mV)	EE (%)	DL (%)	Key characteristics
Thin-film hydration	Quercetin	1:40	113	−84.9	96.7	2.36	Improved Que solubility Moderate size
Thin-film hydration	Rutin	1:10	98	−63.1	47.2	4.54	Lower EE Lower size
Ethanol injection	Quercetin	1:20	174	−58.1	28.1	3.47	Low EE Higher particle size
Ethanol injection	Rutin	1:10	75	−60.1	36.9	3.95	Smaller particle size Lower DL
Micro-fluidics	Rutin	1:4	160	−61.0	37.5	11.10	Highest DL% Higher size

– we carried out DSC experiments to identify the possible interactions between the lipid-based carrier and the encapsulated drugs. The thermograms were normalized between 0 and 1 due to the great endothermic peak of Que (see **Fig. S6A**), which would have suppressed the sign of the formulation and Aso. Fig. 6A shows that the curve of Aso is rather complicated, and only wide peaks can be seen since it is a mixture of multiple compounds, which makes it hard to identify each peak. The case of Que is much simpler; the loss of crystal water can be observed at 126 °C, while the sharp endothermic signal at 326 °C can be attributed to the melting point of Que [42]. When the curve of the formulation (TFH) is analyzed, the most obvious change in the graph is the loss of the first peak of Que and a sharp decrease in the broad peak at 335 °C. The drug-carrier interaction may be the cause of this melting point shift.

In the case of Rut (Fig. 6B), the same two endothermic peaks are dominant in the DSC thermograms: at 138 °C the loss of crystal water and at 173 °C the melting point can be seen [43]. The DSC thermogram of the purified Aso differs from that of the unpurified Aso; however, it is still hard to tell which peak can be attributed to which process. The peak between 250 and 350 °C is in good linear match with the DPPC (dipalmitoyl phosphatidyl choline) content of Aso. From the DSC curve of the formulation (MF), we could conclude that the double peak of pAso at 170 and 174 °C and the melting point of Rut overlap; however, all of them disappear and supposedly merge into one broader peak at 174 °C on the curve of the formulation. The disappearance of the melting point of Rut might be due to the loss of its crystalline state. As a reference measurement, the physical mixture of Rut and pAso was also examined by DSC (**Fig. S6D**), in which the crystal water loss of Rut and the double endothermic peak of pAso can be seen, which further strengthens the supposition that Rut is encapsulated in the particles.

Infrared spectroscopic measurements were performed for the lyophilized samples as well. Fig. 7 shows the spectra of the drugs, the unpurified (in the case of Que) and purified (for Rut) Aso, and the formulations.

The IR spectra were normalized and shifted to see the changes of the different peaks and presented in the 600–1800 cm^{-1} region (the full spectra are presented in **Fig. S7**). The first obvious observation that we can make is that the pure drugs have many sharp peaks, which can be due to their pure crystalline form. Moreover, these many sharp peaks are due to the orderliness and structural complexity of the molecule. In contrast, the IR spectrum of Aso has much wider and significantly fewer peaks, which can be the consequence of its many components (*e.g.,* phosphatidylcholine, phosphatidylserine, phosphatidylethanolamine, phosphatidylinositol, *etc.* [22]). When it comes to the examination of the formulated Que with the thin-film hydration (TFH) method (Fig. 7A), we can see that 2 small peaks appear in the spectrum of the particles, at 1170 cm^{-1} and 1319 cm^{-1}. The first peak can be attributed to the backbone of the flavonoid (C-CO-C skeleton), while the latter peak indicates the presence of the in-plane bending of C—H bonds in aromatic systems [44].

In the case of the formulated Rut with the microfluidic (MF) method (Fig. 7B), a lot more peaks of Rut seem to appear in the spectrum of the formulation, which might be due to the fact that in this case higher DL% value could be achieved. At ~812 cm^{-1} the 'oop' (out-of-plane) bend of C—H bond (in aromatics) appears in the spectrum of the formulation and changes the shape of the peak of Aso. Also, at ~994 cm^{-1} the = C-H bend can be seen, which gives a small shoulder to the high peak of Aso. Also, the peak of the ether bond with the sugar moiety at 1203 cm^{-1}, the peak of the C—O bond at 1363 cm^{-1}, the C—C bond (in aromatic systems) at 1593 cm^{-1} and the O—H deformation vibration at 1658 cm^{-1} [45] all appear in the spectrum of the formulation. All these observations suggest that the encapsulation of the drugs was successful, however since shifts of these peaks cannot be largely seen, we can suggest that only weak forces (supposedly hydrophobic interactions or H-bonds) can lead to the encapsulation.

3.4. *In vitro release studies*

After the characterization of the individual materials, as a last step of the study we planned to carry out the examination of the dissolution of the drugs from the produced carriers. Fig. 8A and B show the dissolution profiles of the pure and formulated Que and Rut, respectively. Firstly, in the case of Que (Fig. 8A) a delay can be seen in the dissolution, which can be explained with the poor water solubility of this compound, which is further strengthened by the fact that after 360 min, only 36.5% of Que could penetrate the membrane. However, with the formulation, we could reduce the retention of Que, since a faster dissolution was achieved even at the early stage of the experiment. Moreover, after 360 min, a higher amount of the drug was able to dissolve (53.7%) than without formulation.

In the case of Rut (Fig. 8B), complete dissolution can be seen, which can be due to its higher solubility. When compared to the dissolution profile of the formulated drug, we can conclude that the formulation can still result in complete dissolution, however, the retention of the drug is only achieved to a very small extent. The DSC thermograms suggest that the melting points of the pure drugs (Que and Rut) are either shifted or disappear in the formulations, which can mean that they lost their crystalline state. Since the dissolution of amorphous materials is much faster than that of ones with a crystalline state (due to the lack of breaking the crystal structure), this phenomenon could be expected in the case of the formulations as well. This amorphous state could be the

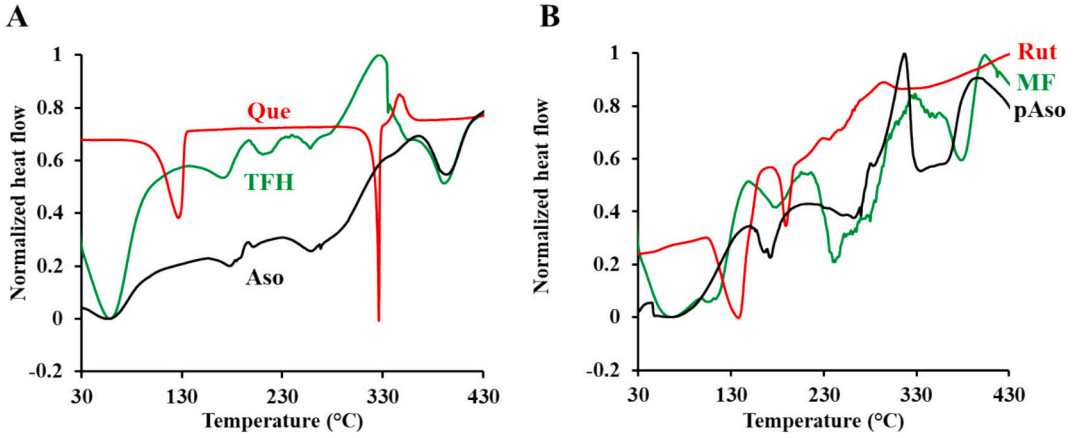

Fig. 6. DSC thermograms of the pure drugs (Que, Rut), the carriers (Aso, pAso), and the formulations prepared by different methods: (**A**) Que, Aso and the formulation created by thin-film hydration (TFH) method; and (**B**) Rut, pAso and the formulation created by the microfluidic (MF) method. All cases solid samples were measured.

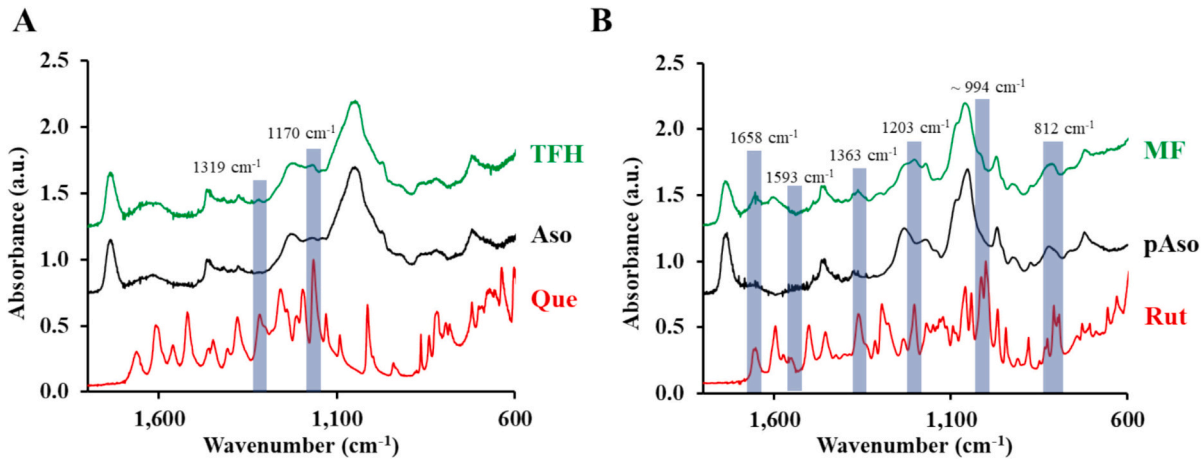

Fig. 7. The FT-IR spectra of the drugs (Que, Rut), the carriers (Aso, pAso) and the formulations in the case of (**A**) Que and the thin-film hydration (TFH) method; and (**B**) Rut and the microfluidic (MF) method (solid samples).

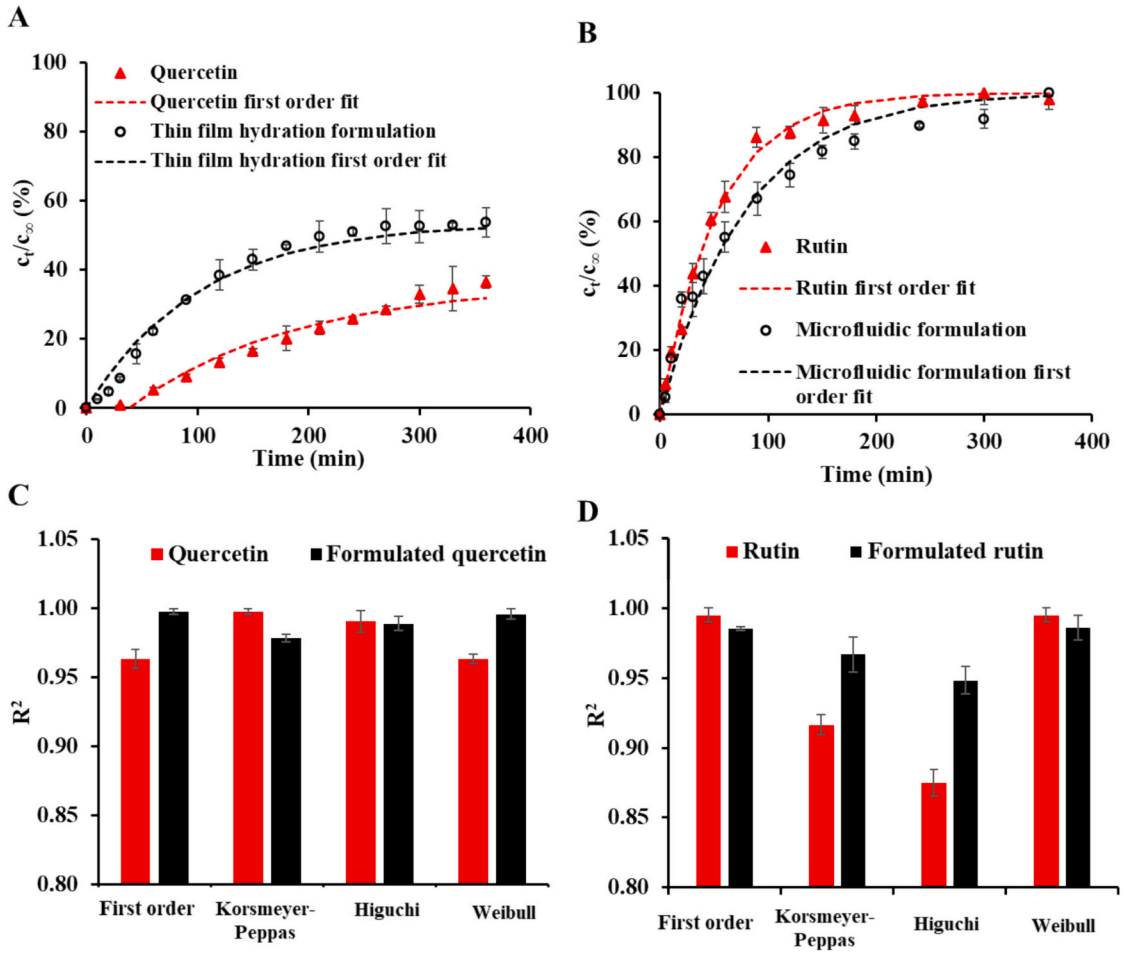

Fig. 8. The dissolution profiles of (**A**) Que and (**B**) Rut from the prepared dispersions (○) and their pure form (▲) in PBS (pH = 7.4, 0.9% NaCl, 2.5 mg/mL Tween80, T = 37 °C). The dashed lines represent the fits with the first order kinetic model. The R^2 values of the fits with different kinetic models for (**C**) Que and (**D**) Rut containing systems.

reason for the faster release of Que; however, this phenomenon cannot be seen in the case of Rut, possibly due to its better water solubility and more hydrophilic nature. This is why the release curve of the formulation and the pure Rut is almost the same.

In order to interpret the results of the dissolution studies more deeply, the measured data were fitted with different frequently used kinetic models (first-order, Korsmeyer-Peppas, Higuchi, and Weibull) (see **Fig. S8 and S9**). To get an initial insight into which model is the best for the description of the dissolution, the R^2 values (Fig. 8C, D) of the fits are analyzed.

For Que, every model showed R^2 > 0.95. For pure drug, the Korsmeyer-Peppas (R^2 = 0.9978) and the Higuchi (R^2 = 0.9904) gave

Table 3
The fitting parameters of the dissolution curves using the first-order, Korsmeyer-Peppas, Higuchi and Weibull models.

Model		Quercetin	Thin-film hydration formulation	Rutin	Flow system formulation
First order model	k (min^{-1})	0.0065	0.0099	0.0189	0.0129
	$t_{1/2}$ (min)	107.4	70.1	36.8	53.8
	T (min)	36.9	–	–	–
	R^2	0.9633	0.9978	0.9952	0.9855
Korsmeyer-Peppas model	k_m (min^{-n})	1.176	1.653	0.1376	0.0994
	n	0.7713	0.7663	0.3583	0.4023
	T (min)	34.6	–	–	–
	R^2	0.9978	0.9781	0.9166	0.9668
Higuchi model	k ($min^{-1/2}$)	5.015	5.779	0.0658	0.0597
	T (min)	32.6	–	–	–
	R^2	0.9904	0.9890	0.8750	0.9483
Weibull model	a	4.190	7.681	0.4770	0.4742
	b	0.0270	0.0760	0.0090	0.0061
	T (min)	36.9	–	–	–
	R^2	0.9633	0.9958	0.9952	0.9861

the best fits, while for the formulation, the first order ($R^2 = 0.9978$) and Weibull models ($R^2 = 0.9958$) seemed to describe the dissolution best. In the case of Rut, the first-order and Weibull models were the best for the description of the drug release for both the pure and the formulated compounds. When it comes to the analysis of the fitting parameters (Table 3), we can compare the half-life and rate constant values of the first-order model fits. In the case of Que, the k value increases upon formulation, and the half-life decreases from 107 min to 70 min, which also indicates that formulation can enhance the dissolution of the drug. The n parameter of the Korsmeyer-Peppas model can show what controls the dissolution ($n = 0.5$ – diffusion control, $n = 1$ – erosion control). The values obtained from the fits ($n = 0.77$ and $n = 0.76$ for the pure and formulated drug, respectively) suggest that the dissolutions are controlled by both diffusion and erosion. Also, we can see that the dissolution is best described by the Higuchi and Korsmeyer-Peppas models, while for the formulation, these models give the worst fits. For every model, the delay time in the case of Que happens to be between 32.6 and 36.9 min.

In the case of the dissolution of Rut, we can see that the formulation increases the half-life of the drug release, while the rate constant increases to a small extent, as the first-order model suggests. The low n values of the Korsmeyer-Peppas model ($n = 0.35$ and $n = 0.40$) mean that the dissolution of the pure and formulated rutin is diffusion controlled. For the release of Rut, the Higuchi model seemed to give the worst fit in every case.

Since the Weibull model is a semiempirical model, it can fit most dissolution profiles well; this is why the only conclusion we can make from this model is that in most cases, this gave the best fit. Moreover, its close R^2 value to the first-order model further strengthens the goodness of the first-order model.

4. Conclusion

In this work, asolectin-based colloidal systems were systematically developed and evaluated as carriers for two structurally related flavonoids, Que and Rut, using TFH, ethanol injection, and microfluidic preparation routes. No similar publication was available in the literature regarding the formulation of these compounds in the carrier we chose. By applying identical lipid matrices and comparable formulation conditions, the study enabled a direct assessment of how molecular structure, solubility, and preparation pathways govern self-assembly, intermolecular interactions, and macroscopic performance of lipid particles.

All preparation methods yielded stable, negatively charged colloidal dispersions with ~150 nm hydrodynamic diameters; however, pronounced differences were observed in encapsulation behavior and attainable drug loading. Que, characterized by its hydrophobic aglycone structure, showed strong affinity toward the lipid phase, leading to exceptionally high encapsulation efficiencies (>90%) when prepared by thin-film hydration. In contrast, the more hydrophilic Rut, bearing a disaccharide moiety, exhibited lower encapsulation efficiencies but substantially higher drug loading when formulated by microfluidic mixing, highlighting the critical role of controlled solvent exchange and self-assembly kinetics at the molecular level.

Thermal and spectroscopic analyses confirmed the successful incorporation of both flavonoids into the asolectin matrix and indicated that the encapsulation is driven predominantly by weak, non-covalent interactions, such as hydrophobic forces and hydrogen bonding, rather than by the formation of new crystalline or strongly bound phases. These findings are consistent with the observed release behavior: Que formulation resulted in enhanced dissolution and accelerated release kinetics, whereas Rut release remained largely diffusion-controlled, reflecting its higher intrinsic solubility and weaker partitioning into the lipid domain.

Overall, the results demonstrate that subtle differences in flavonoid molecular architecture translate into distinct colloidal organization, loading capacity, and release dynamics within lipid-based carrier systems. From the perspective of molecular liquids and colloidal science, this study underscores the importance of preparation-induced self-assembly pathways and solute–lipid interactions in determining the structure–property relationships of complex liquid dispersions. The insights gained here provide a rational basis for tailoring lipid-based delivery systems for poorly soluble bioactive compounds and contribute to a deeper molecular-level understanding of surfactant-driven colloidal systems relevant to pharmaceutical and nutraceutical applications. In our opinion, the experimental results can be successfully used for the formulation design of compounds with similar structure and solubility.

CRediT authorship contribution statement

Virág Viktória Kiss: Methodology, Investigation. **Norbert Varga:** Methodology, Investigation. **Ádám Juhász:** Methodology, Investigation. **László Seres:** Writing – original draft, Visualization, Methodology, Investigation. **Edit Csapó:** Writing – review & editing, Writing – original draft, Supervision, Project administration, Conceptualization.

Informed consent statement

Not applicable.

Institutional review board statement

Not applicable.

Declaration of competing interest

The authors declare that they have no known competing financial interests or personal relationships that could have appeared to influence the work reported in this paper.

Acknowledgements

TKP2021-EGA-32 has been implemented with the support provided by the Ministry of Innovation and Technology of Hungary from the National Research, Development and Innovation Fund. L.S. thanks the financial support of the Research Fellowship Program (EKÖP-511-SZTE) of the Ministry of Culture and Innovation from the National Fund for Research, Development and Innovation. The publication was also funded by the University of Szeged Open Access Fund (FundRef, Grant No. 8568).

Appendix A. Supplementary data

Supplementary data to this article can be found online at https://doi.org/10.1016/j.molliq.2026.129530.

Data availability

Data is contained within the article and supplementary material. More data are available on request.

References

[1] A.N. Panche, A.D. Diwan, S.R. Chandra, Flavonoids: an overview, Journal of Nutritional, Science 5 (2016) e47, https://doi.org/10.1017/jns.2016.41.
[2] V. D'Amelia, R. Aversano, P. Chiaiese, D. Carputo, The antioxidant properties of plant flavonoids: their exploitation by molecular plant breeding, Phytochem. Rev. 17 (2018) 611–625, https://doi.org/10.1007/s11101-018-9568-y.
[3] S.J. Maleki, J.F. Crespo, B. Cabanillas, Anti-inflammatory effects of flavonoids, Food Chem. 299 (2019) 125124, https://doi.org/10.1016/j.foodchem.2019.125124.
[4] A. Al Hoque, S. Begum, D. Dutta, Occurrence, Chemical Nature, and Medicinal Benefits of Flavonoids: Rutin, Kaempferol, Quercetin, Anthocyanidins, Catechins, and Flavones, in: Dietary Supplements and Nutraceuticals, Springer, Singapore, 2025, pp. 185–208, https://doi.org/10.1007/978-981-96-8622-3_5.
[5] S. Zhou, X. Qingman, W. Zhang, D. Zhang, S. Liu, Quercetin as a Multi-Target Natural Therapeutic in Aging-Related Diseases: Systemic Molecular and Cellular Mechanisms, Phytother. Res. 39 (2025) 4821–4869, https://doi.org/10.1002/ptr.70078.
[6] N. Lu, Y. Ding, Z. Yang, P. Gao, Effects of rutin on the redox reactions of hemoglobin, Int. J. Biol. Macromol. 89 (2016) 175–180, https://doi.org/10.1016/j.ijbiomac.2016.04.066.
[7] J.A. Rothwell, A.J. Day, M.R.A. Morgan, Experimental Determination of Octanol−Water Partition Coefficients of Quercetin and Related Flavonoids, J. Agric. Food Chem. 53 (2005) 4355–4360, https://doi.org/10.1021/jf0483669.
[8] H.-M. Li, T.-T. Xu, Q.-X. Peng, Y.-S. Chen, H. Zhou, Y.-Y. Lu, R.-A. Yan, Enzymatic acylation of rutin with benzoic acid ester and lipophilic, antiradical, and antiproliferative properties of the acylated derivatives, J. Food Sci. 86 (2021) 1714–1725, https://doi.org/10.1111/1750-3841.15703.
[9] A. Naeem, Y. Ming, H. Pengyi, K.Y. Jie, L. Yali, Z. Haiyan, X. Shuai, L. Wenjing, W. Ling, Z.M. Xia, L.S. Shan, Z. Qin, The fate of flavonoids after oral administration: a comprehensive overview of its bioavailability, Crit. Rev. Food Sci. Nutr. 62 (2022) 6169–6186, https://doi.org/10.1080/10408398.2021.1898333.
[10] R. Abdi Syahputra, A. Dalimunthe, Z.D. Utari, P. Halim, M.A. Sukarno, S. Zainalabidin, E. Salim, M. Gunawan, F. Nurkolis, M.N. Park, J.A. Luckanagul, H. Bangun, B. Kim, U. Harahap, Nanotechnology and flavonoids: Current research and future perspectives on cardiovascular health, J. Funct. Foods 120 (2024) 106355, https://doi.org/10.1016/j.jff.2024.106355.
[11] Ya.F. Zverev, A.Ya. Rykunova, Modern Nanocarriers as a Factor in Increasing the Bioavailability and Pharmacological Activity of Flavonoids, Appl. Biochem. Microbiol. 58 (2022) 1002–1020, https://doi.org/10.1134/S0003683822090149.
[12] Z. Chenxi, A. Hemmat, N. Thi, M. Afrand, Nanoparticle-enhanced drug delivery systems: An up-to-date review, J. Mol. Liq. 424 (2025) 126999, https://doi.org/10.1016/j.molliq.2025.126999.
[13] A. Ilyas, G. Abbas, S. Shah, M.M.Z. Javaid, M. Iqbal, A. Mahmood, A. Rasul, A. Fatima, M. Tahir, N.I. Namazi, Polymeric nanocomposites of flavonoids with pectin for ocular delivery of an antibiotic drug, J. Mol. Liq. 433 (2025) 127806, https://doi.org/10.1016/j.molliq.2025.127806.
[14] A. Rezaei, M. Fathi, S.M. Jafari, Nanoencapsulation of hydrophobic and low-soluble food bioactive compounds within different nanocarriers, Food Hydrocoll. 88 (2019) 146–162, https://doi.org/10.1016/j.foodhyd.2018.10.003.
[15] F. Kayaci, T. Uyar, Encapsulation of vanillin/cyclodextrin inclusion complex in electrospun polyvinyl alcohol (PVA) nanowebs: Prolonged shelf-life and high temperature stability of vanillin, Food Chem. 133 (2012) 641–649, https://doi.org/10.1016/j.foodchem.2012.01.040.
[16] Z. Aytac, S.I. Kusku, E. Durgun, T. Uyar, Quercetin/β-cyclodextrin inclusion complex embedded nanofibres: Slow release and high solubility, Food Chem. 197 (2016) 864–871, https://doi.org/10.1016/j.foodchem.2015.11.051.
[17] M. Colombo, L.R. Michels, H.F. Teixeira, L.S. Koester, Flavonoid delivery by solid dispersion: a systematic review, Phytochem. Rev. 21 (2022) 783–808, https://doi.org/10.1007/s11101-021-09763-3.
[18] S. Khaledian, M. Dayani, A. Fatahian, R. Fatahian, F. Martinez, Efficiency of lipid-based nano drug delivery systems in crossing the blood–brain barrier: A review, J. Mol. Liq. 346 (2022) 118278, https://doi.org/10.1016/j.molliq.2021.118278.
[19] M. Peruš, M. Knez Marevci, P. Kotnik, Liposomes: recent progress on nanoparticles production and their usage in medicine, Biomater. Adv. 180 (2026) 214585, https://doi.org/10.1016/j.bioadv.2025.214585.
[20] R.S. de Sousa, A.O. de Moraes Nogueira, V.G. Marques, R.M. Clementin, V.R. de Lima, Effects of α-eleostearic acid on asolectin liposomes dynamics: Relevance to its antioxidant activity, Bioorg. Chem. 51 (2013) 8–15, https://doi.org/10.1016/j.bioorg.2013.08.004.
[21] S.E. Mansoor, K. Palczewski, D.L. Farrens, Rhodopsin self-associates in asolectin liposomes, Proc. Natl. Acad. Sci. 103 (2006) 3060–3065, https://doi.org/10.1073/pnas.0511010103.
[22] A. Johns, S. Morris, K. Edwards, R.L. Quirino, Asolectin from soybeans as a natural compatibilizer for cellulose-reinforced biocomposites from tung oil, J. Appl. Polym. Sci. 132 (2015), https://doi.org/10.1002/app.41833.
[23] Y. Jiang, W. Li, Z. Wang, J. Lu, Lipid-Based Nanotechnology: Liposome, Pharmaceutics 16 (2023) 34, https://doi.org/10.3390/pharmaceutics16010034.
[24] M. Mehta, T.A. Bui, X. Yang, Y. Aksoy, E.M. Goldys, W. Deng, Lipid-Based Nanoparticles for Drug/Gene Delivery: An Overview of the Production Techniques and Difficulties Encountered in Their Industrial Development, ACS Mater. Au 3 (2023) 600–619, https://doi.org/10.1021/acsmaterialsau.3c00032.
[25] A. Akbarzadeh, R. Rezaei-Sadabady, S. Davaran, S.W. Joo, N. Zarghami, Y. Hanifehpour, M. Samiei, M. Kouhi, K. Nejati-Koshki, Liposome: classification, preparation, and applications, Nanoscale Res. Lett. 8 (2013) 102, https://doi.org/10.1186/1556-276X-8-102.
[26] G. Du, X. Sun, Ethanol Injection Method for Liposome Preparation, in: G.G. M. D'Souza, H. Zhang (Eds.), Liposomes: Methods and Protocols, Springer US, New York, NY, 2023, pp. 65–70, https://doi.org/10.1007/978-1-0716-2954-3_5.
[27] R. Yang, X. Zhang, J. Si, X. Zhao, J. Song, Liposome Technology in Food Science: Structure, Preparation Techniques, and Functional Applications, J. Fut. Foods (2025), https://doi.org/10.1016/j.jfutfo.2025.11.003.
[28] D. Carugo, E. Bottaro, J. Owen, E. Stride, C. Nastruzzi, Liposome production by microfluidics: potential and limiting factors, Sci. Rep. 6 (2016) 25876, https://doi.org/10.1038/srep25876.
[29] M.J. Javid-Naderi, S.A. Mousavi Shaegh, Advanced microfluidic techniques for the preparation of solid lipid nanoparticles: Innovations and biomedical applications, Int. J. Pharm. X 10 (2025) 100399, https://doi.org/10.1016/j.ijpx.2025.100399.
[30] I. Erlund, T. Kosonen, G. Alfthan, J. Mäenpää, K. Perttunen, J. Kenraali, J. Parantainen, A. Aro, Pharmacokinetics of quercetin from quercetin aglycone and rutin in healthy volunteers, Eur. J. Clin. Pharmacol. 56 (2000) 545–553, https://doi.org/10.1007/s002280000197.
[31] S. Andres, S. Pevny, R. Ziegenhagen, N. Bakhiya, B. Schäfer, K.I. Hirsch-Ernst, A. Lampen, Safety Aspects of the Use of Quercetin as a Dietary Supplement, Mol. Nutr. Food Res. 62 (2018) 1700447, https://doi.org/10.1002/mnfr.201700447.
[32] S. Sharma, J.K. Sahni, J. Ali, S. Baboota, Patent Perspective for Potential Antioxidant Compounds-Rutin and Quercetin, Recent Patents on, Nanomedicine 3 (2013) 62–68, https://doi.org/10.2174/18779123112029990002.
[33] S. Sharma, A. Ali, J. Ali, J.K. Sahni, S. Baboota, Rutin: therapeutic potential and recent advances in drug delivery, Expert Opin. Investig. Drugs 22 (2013) 1063–1079, https://doi.org/10.1517/13543784.2013.805744.
[34] Y. Wu, T. Wang, Fractionation of crude soybean lecithin with aqueous ethanol, J. Am. Oil Chem. Soc. 81 (2004) 697–704, https://doi.org/10.1007/s11746-004-964-x.
[35] M. Sosada, Optimal conditions for fractionation of rapeseed lecithin with alcohols, J. Am. Oil Chem. Soc. 70 (1993) 405–410, https://doi.org/10.1007/BF02552715.
[36] V.V. Patil, R.V. Galge, B.N. Thorat, Extraction and purification of phosphatidylcholine from soyabean lecithin, Sep. Purif. Technol. 75 (2010) 138–144, https://doi.org/10.1016/j.seppur.2010.08.006.
[37] S. Mabrey, J.M. Sturtevant, Investigation of phase transitions of lipids and lipid mixtures by sensitivity differential scanning calorimetry, Proc. Natl. Acad. Sci. 73 (1976) 3862–3866, https://doi.org/10.1073/pnas.73.11.3862.
[38] A. Blume, Thermotropic behavior of phosphatidylethanolamine-cholesterol and phosphatidylethanolamine-phosphatidylcholine-cholesterol mixtures, Biochemistry 19 (1980) 4908–4913, https://doi.org/10.1021/bi00562a032.
[39] Á. Juhász, D. Ungor, K. Berta, L. Seres, E. Csapó, Spreadsheet-based nonlinear analysis of in vitro release properties of a model drug from colloidal carriers, J. Mol. Liq. 328 (2021) 115405, https://doi.org/10.1016/j.molliq.2021.115405.

[40] I.G. Zenkevich, S.V. Guschina, Determination of dissociation constants of species oxidizable in aqueous solution by air oxygen on an example of quercetin, J. Anal. Chem. 65 (2010) 371–375, https://doi.org/10.1134/S1061934810040064.
[41] K. Srinivas, J.W. King, L.R. Howard, J.K. Monrad, Solubility and solution thermodynamic properties of quercetin and quercetin dihydrate in subcritical water, J. Food Eng. 100 (2010) 208–218, https://doi.org/10.1016/j.jfoodeng.2010.04.001.
[42] T. Muthurajan, P. Rammanohar, N.P. Rajendran, S. Sethuraman, U.M. Krishnan, Evaluation of a quercetin–gadolinium complex as an efficient positive contrast enhancer for magnetic resonance imaging, RSC Adv. 5 (2015) 86967–86979, https://doi.org/10.1039/C5RA16405B.
[43] C.M.S. Neto, F.C. Lima, R.P. Morais, L.R.M. de Andrade, R. de Lima, M.V. Chaud, M.M. Pereira, R.L.C. de A. Júnior, J.C. Cardoso, A. Zielińska, E.B. Souto, Á.S. Lima, P. Severino, Rutin-functionalized multi-walled carbon nanotubes: molecular docking, physicochemistry and cytotoxicity in fibroblasts, Toxics 9 (2021). doi: https://doi.org/10.3390/toxics9080173.
[44] M. Catauro, F. Papale, F. Bollino, S. Piccolella, S. Marciano, P. Nocera, S. Pacifico, Silica/quercetin sol–gel hybrids as antioxidant dental implant materials, Sci. Technol. Adv. Mater. 16 (2015) 035001, https://doi.org/10.1088/1468-6996/16/3/035001.
[45] I.M. Savic, I.M. Savic-Gajic, V.D. Nikolic, L.B. Nikolic, B.C. Radovanovic, A. Milenkovic-Andjelkovic, Enhencemnet of solubility and photostability of rutin by complexation with β-cyclodextrin and (2-hydroxypropyl)-β-cyclodextrin, J. Incl. Phenom. Macrocycl. Chem. 86 (2016) 33–43, https://doi.org/10.1007/s10847-016-0638-8.